

Unconventional Quantum Electrodynamics with Hofstadter-Ladder Waveguide

Xin Wang,¹ Zhao-Min Gao,¹ Jia-Qi Li,¹ Huai-Bing Zhu,¹ and Hong-Rong Li¹

¹*Institute of Theoretical Physics, School of Physics,
Xi'an Jiaotong University, Xi'an 710049, People's Republic of China*

(Dated: October 6, 2022)

We propose a novel quantum electrodynamics (QED) platform where quantum emitters interact with a Hofstadter-ladder waveguide. We demonstrate several intriguing phenomena stemming from the nontrivial dispersion relation and vacuum mode properties led by the effective spin-orbit coupling. First, by assuming emitter's frequency to be resonant with the lower band, we find that the spontaneous emission is chiral with most photonic field decaying unidirectionally. Both numerical and analytical results indicate that the Hofstadter-ladder waveguide can be engineered as a well-performed chiral quantum bus. Second, the dynamics of emitters of giant atom form is explored by considering their frequencies below the lower band. Due to quantum interference, we find that both the emitter-waveguide interaction and the amplitudes of bound states are periodically modulated by giant emitter's size. The periodical length depends on the positions of energy minima points induced by the spin-orbit coupling. Last, we consider the interaction between two giant emitters mediated by bound states, and find that their dipole-dipole interaction vanishes (is enhanced) when maximum destructive (constructive) interference happens.

I. INTRODUCTION

The interactions between quantum emitters and the unavoidable baths with large degrees of freedom are the central topic of quantum optics [1, 2]. For example, in the present of a vacuum bath, the emitter will spontaneously decay to its ground state as well as its frequency being renormalized due to Lamb shifts [3, 4]. By shaping the size of the environment or narrowing its spectrum bandwidth, many intriguing phenomena, such as isotropic propagation of photons and non-Markovian evolution arise [5–10]. As discussed in Refs. [11–15], chiral emission can be observed via the subwavelength confinement in nanophotonic systems, which opens the possibilities to realize cascaded quantum networks. Moreover, when considering an emitter coupling to the bandgaps of a bath [16–22], photonic bound states (in the form of an evanescent field) emerge [23]. In this scenario, between atoms there are long-range dipole-dipole interactions by exchanging the virtual photons in the waveguide [24, 25].

In recent years, exploring quantum electrodynamics (QED) with emitters coupling to structured lattice environments, has attracted a lot of interests [26–30]. Those artificial lattice reservoirs are widely studied in condensed matter physics, and usually have unconventional spectra, or topological properties with nontrivial vacuum modes. In Refs. [31, 32], by considering emitters interacting with a 2D tight-binding lattice environment, the authors showed that both superradiance and subradiance of collective atoms emerge in the nonperturbative regime. The unusual chiral bound states and directional dipole-dipole interaction were also demonstrated in a topological waveguide QED system [33, 34]. In Refs. [35, 36], the authors discussed how to realize bound states and dipole-dipole interactions in non-Hermitian photonic lattices. All these studies indicate those structured lattice reservoirs with reduced

dimensionality are versatile toolboxes for exploring novel quantum optical phenomena, as well as the potential applications in quantum information processing.

In artificial baths with the spin-orbit coupling, the motion and spin freedoms of a particle are linked, and many anomalous phenomena such as spin-Hall effect and topological insulators can be observed [37–47]. Since neither the spin nor the momentum is the well-defined quantum number to describe the dispersion relation, the spin-orbit coupling will produce nontrivial energy bands and photonic modes [48, 49]. The quantum optics with emitters interacting with baths of the spin-orbit coupling, is rarely studied. It is a simple but interesting toy model in condensed matter physics (see Fig. 1) [50–56]. As discussed in Ref. [57], the ladder contains two legs which play the roles of two freedoms in an effective spin. In the present of synthetic gauge fields, the effective spin will be locked to momentum freedom.

In this work, we discuss QED phenomena in a setup composed by quantum emitters and a Hofstadter-ladder waveguide. Different from previous studies based on lattice environment with synthetic gauge fields [58–61], here we mainly focus on unconventional QED phenomena induced by the spin-orbit coupling. First, we assume that the emitter is of small atom form which frequency is resonant with the lower energy band. Due to spin-momentum locking, the emitter chirally dissipates almost all its energy into one direction of the waveguide, which is different from the directional emission along the edge states of a 2D topologically nontrivial lattice [62]. In our study the chiral emission into the 1D Hofstadter-ladder waveguide stems from the effective spin-orbit coupling, and does not require any topological protection. Our proposal is possible to demonstrate chiral quantum optics, which has been extensively studied in Refs. [63–67]. Second, the emitter is considered as giant atom form, and couples to the waveguide at multiple sites [68–77]. Given that emitters'

frequency is below two degenerate minima points induced by the spin-orbit coupling, there will be bound state in which the photonic energy will be trapped. The bound state induced by time-delay effects of giant atom has been investigated in Ref. [78]. In this work, we focus on another giant atom effect, i.e., the quantum interference between different coupling points. We find that, due to quantum interference and unconventional spectrum of the Hofstadter-ladder waveguide, the bound state will be periodically modulated by the giant atom's size. The periodical length is tunable by controlling the parameters of the Hofstadter ladder waveguide. Based on this mechanism, we show that by tuning the interference as constructive/destructive, the dipole-dipole interaction between two giant emitters will be enhanced/suppressed.

II. SPECTRUM AND SPIN-ORBIT COUPLING OF HOFSTADTER-LADDER WAVEGUIDE

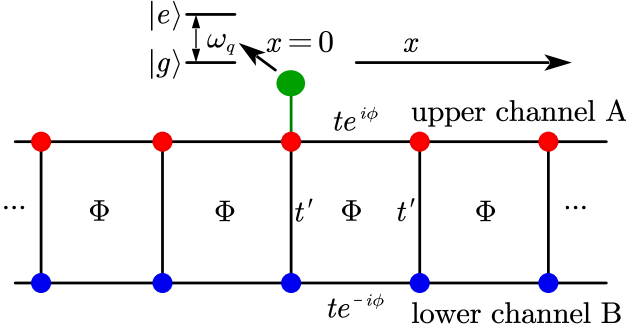


FIG. 1. A two-level quantum emitter interacts with a waveguide in the form of the photonic analog of a Hofstadter-ladder model. The ladder rungs are hopped with strength t' . The nearest neighbor sites in two legs are coupled at rate t , together with a synthetic gauge phase $e^{i\phi}$ ($e^{-i\phi}$) for channel A (B). The effective magnetic field through each plaquette is $\Phi = 2\phi$.

The model of the QED setup we study is depicted in Fig. 1, where a quantum emitter interacts with an artificial one-dimensional waveguide along the x direction, which behaves as a photonic analog of the Hofstadter-ladder model. The Hofstadter ladder can be viewed as the two-leg edge of the Harper-Hofstadter model [79], where a synthetic gauge field $\Phi = 2\phi$ is applied through each plaquette (see Fig. 1). Here we consider it working as a 1D artificial waveguide which allows photons traveling along it. In this situation, two legs in of the ladder waveguide serve as channel A and B of the waveguide. For convenience, we set the length of one unit site as $d_0 = 1$. The ladder waveguide is composed by two legs, which can be viewed as two quantum channels for the emitter. Two sites in each rung are coupled with strength t' , which is set as $t' = 1$. By adopting a Landau gauge along the x direction, the

phase connections only appear in each leg. Therefore, the hopping amplitude between two nearest neighbor sites is $te^{i\phi}$ ($te^{-i\phi}$) for channel A (B). Consequently, by setting $\hbar = 1$, the tight-binding Hamiltonian of the waveguide is [56]

$$H_B = \sum_x \omega_0 (a_x^\dagger a_x + b_x^\dagger b_x) - \left[t' \sum_x a_x^\dagger b_x + t \sum_x \left(e^{i\phi} a_{x+1}^\dagger a_x + e^{-i\phi} b_{x+1}^\dagger b_x \right) + \text{H.c.} \right], \quad (1)$$

where a_x, b_x (a_x^\dagger, b_x^\dagger) are the annihilation (creation) operators of the sites a, b at position x , and ω_0 is the identical frequency of those bosonic modes. In the following we work in the rotating frame of the constant part $\sum_x \omega_0 (a_x^\dagger a_x + b_x^\dagger b_x)$.

Under the periodic boundary condition and in the momentum space with

$$a_k^\dagger = \frac{1}{\sqrt{N}} \sum_x e^{ikx} a_x^\dagger, \quad b_k^\dagger = \frac{1}{\sqrt{N}} \sum_x e^{ikx} b_x^\dagger, \\ k = \frac{2\pi}{N} n, \quad n \in (-N/2, N/2], \quad (2)$$

we can diagonalize the waveguide Hamiltonian as

$$H_B = -2t \begin{bmatrix} a_k^\dagger & b_k^\dagger \end{bmatrix} \mathcal{H}_B \begin{bmatrix} a_k \\ b_k \end{bmatrix}, \\ \mathcal{H}_B = \begin{bmatrix} g(k) + f(k) & \eta \\ \eta & g(k) - f(k) \end{bmatrix} \\ = g(k) I + f(k) \sigma_z + \eta \sigma_x, \quad (3)$$

where $\eta = t'/2t$, $g(k)$ and $f(k)$ are respectively expressed as

$$g(k) = \cos \phi \cos k, \quad f(k) = \sin \phi \sin k. \quad (4)$$

As shown in Eq. (3), the Hamiltonian H_B is expressed in the Pauli operators, indicating that the upper-lower leg degree of freedom behaves as an effective spin. Due to the synthetic gauge field, H_B contains the effective spin-orbit coupling term $(\sin \phi \sin k) \sigma_z$, which will lead to spin-momentum locking [57]. Note that in condensed matter physics the concept of “spin” is extensively used for models consisting of “A” and “B” sublattices. Similarly, the spin-orbit coupling is a generalized concept from atomic physics, which describes a two-component internal freedom coupling to the momentum of a particle [79]. For example, in Refs. [48, 80], the spin-orbit coupling and spin Hall insulators for photons have been successfully demonstrated in experiments.

The energy spectrum can be derived by simply diagonalizing \mathcal{H}_B . Consequently, the energy bands and eigenmodes are derived as

$$E_{\pm}(k) = -2t \left[g(k) \mp \sqrt{f^2(k) + \eta^2} \right], \quad (5)$$

$$C_{k-}^\dagger = \begin{pmatrix} \cos \frac{\theta_k}{2} a_k^\dagger & \sin \frac{\theta_k}{2} b_k^\dagger \end{pmatrix}, \quad (6)$$

$$C_{k+}^\dagger = \begin{pmatrix} \sin \frac{\theta_k}{2} a_k^\dagger & -\cos \frac{\theta_k}{2} b_k^\dagger \end{pmatrix}, \quad (7)$$

where $\theta_k = \arctan[\eta/f(k)]$. Now we define the average spin as

$$\langle \sigma_z \rangle_k = \langle a_k^\dagger a_k \rangle - \langle b_k^\dagger b_k \rangle = \cos^2 \frac{\theta_k}{2} - \sin^2 \frac{\theta_k}{2}. \quad (8)$$

Given that $\langle \sigma_z \rangle_k > 0$ ($\langle \sigma_z \rangle_k < 0$), the mode k asymmetrically distributes on channel A (B) with more probabilities. In Fig. 2(a), we plot $E_\pm(k)$ and $\langle \sigma_z \rangle_k$ of two bands versus k . It is found that, due to spin-momentum locking, the chiral current $\langle \sigma_z \rangle_k$ of the lower band is opposite to the upper band for certain momentum k .

Moreover, the spin-orbit coupling significantly modifies the dispersion relation of the waveguide. For a free particle without spin-orbit coupling, the energy minimum point is usually with zero momentum $k = 0$ (or $k = \pm\pi$). When spin-orbit coupling appears, the spin-up and spin-down modes minimize their energies by carrying non-zero opposite momentum k [42]. As depicted in Fig. 2, the photonic dispersion relation of the ladder waveguide becomes spin-dependent, and the energy minima are degenerate at two points with non-zero momentum $k \neq 0$. Moreover, there is Kramers degeneracy for a pair of modes $\pm k$ due to spin-momentum interaction, and the field distribution is mostly localized in channel A (B) for $k > 0$ ($k < 0$) [57]. Those properties allow us to realize unconventional phenomena of quantum optics, which will be addressed in the following discussions.

III. CHIRAL SPONTANEOUS EMISSION

We first consider that the two-energy-level emitter is of small atom form, i.e., couples to the Hofstadter-ladder waveguide at one site $x = 0$ (see Fig. 1). Its frequency lies resonantly within the lower energy band. In the rotating frame of bosonic frequency ω_0 , the system Hamiltonian is written as

$$H_s = H_0 + H_{\text{int}}, \quad (9)$$

$$H_0 = \frac{1}{2} \Delta_q \sigma_z + H_B, \quad H_{\text{int}} = g \left(\sigma_- a_0^\dagger + \sigma_+ a_0 \right), \quad (10)$$

where $\Delta_q = \omega_q - \omega_0$ with ω_q being the emitter's transition frequency, $\sigma_z = |e\rangle\langle e| - |g\rangle\langle g|$ and $\sigma_+ = (\sigma_-)^\dagger = |e\rangle\langle g|$, with $|e\rangle$ ($|g\rangle$) being the excited (ground) state of the emitter. Applying inverse Fourier transform, one obtains $a_0^\dagger = \sum_k a_k^\dagger / \sqrt{N}$. According to Eqs. (6, 7), a_k^\dagger can be decomposed as the superposition of $C_{k\pm}^\dagger$. Finally, the interaction Hamiltonian is written as

$$H_{\text{int}} = \frac{g}{\sqrt{N}} \sum_k \sigma_- \left(\cos \frac{\theta_k}{2} C_{k-}^\dagger + \sin \frac{\theta_k}{2} C_{k+}^\dagger \right) + \text{H.c.} \quad (11)$$

As shown in Fig. 2(a), ω_q is set in the cyan regime, and only the lower band $E_-(k)$ is resonant with the emitter. To avoid the non-Markovian effects led by the band tops [27], we require Δ_q far away from two band edges,

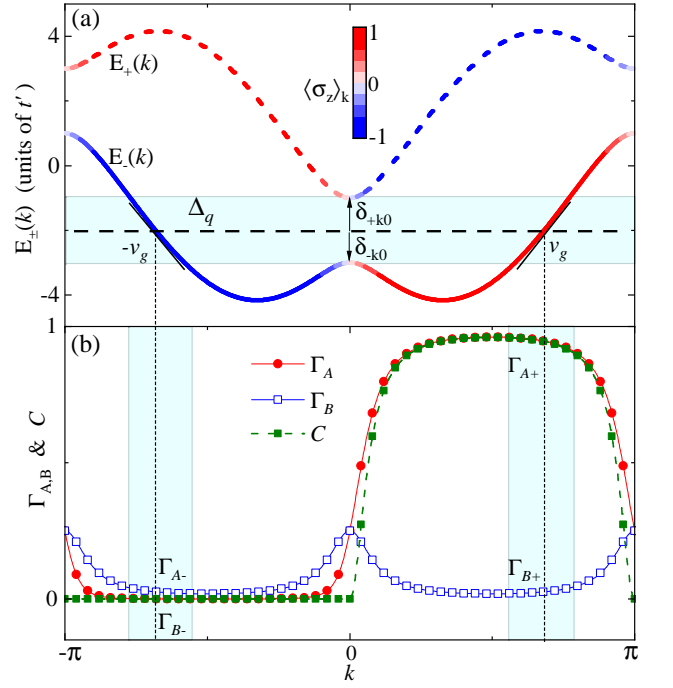


FIG. 2. (a) The dispersion relations for two energy bands of a Hofstadter-ladder waveguide. The effective spin $\langle \sigma_z \rangle_k$ describing the population difference between channel A and B, is mapped with colors. When discussing the chiral emission, the emitter's frequency is assumed in the cyan area, around which the group velocity is v_g . The detuning to the lower (upper) band edge is denoted by δ_{-k0} (δ_{+k0}). (b) The analytical decay rates $\Gamma_{A(B)}$ [in the unit $g^2/(2v_g)$, see Eq. (20)] into channel A (B) and the chiral factor change with k . The cyan area corresponds to the Markovian decay regime where both band edges and the upper energy band do not take apparent effects. The cross points with the dashed vertical lines correspond to the decay rates of the emitter with frequency in (a). Parameters of the whole system: $t' = 1$, $t = 2$ and $\phi = \pi/3$.

i.e., $|\delta_{\pm k0}| \gg 0$. By dropping the off-resonant terms with upper band modes C_{k+}^\dagger , the interacting Hamiltonian is reduced as

$$H_{\text{int}} = \frac{g}{\sqrt{N}} \left(\sum_k \cos \frac{\theta_k}{2} \sigma_- C_{k-}^\dagger + \text{H.c.} \right). \quad (12)$$

After substituting Eq. (6) into Eq. (12), we can divide H_{int} into two parts which describe interactions with channel A and B respectively:

$$H_{\text{int}} = H_{\text{int},A} + H_{\text{int},B}, \quad (13)$$

$$H_{\text{int},A} = \frac{g}{\sqrt{N}} \left(\sum_k \cos^2 \frac{\theta_k}{2} \sigma_- a_k^\dagger + \text{H.c.} \right), \quad (14)$$

$$H_{\text{int},B} = \frac{g}{\sqrt{N}} \left(\sum_k \cos \frac{\theta_k}{2} \sin \frac{\theta_k}{2} \sigma_- b_k^\dagger + \text{H.c.} \right). \quad (15)$$

From Eq. (13) and as depicted in Fig. 2(a), we find four

dissipation terms by assuming the resonant position at $\Delta_q = E_-(\pm k_r)$, i.e., the left/right direction of channel A (B). After applying the unitary transformation $U_0(t) = \exp(-iH_0t)$, the interaction operator with channel A becomes

$$\sum_k (\sigma_- a_k^\dagger) \rightarrow \frac{N}{2\pi} \int_{-\pi}^{\pi} (\sigma_- a_k^\dagger e^{i\Delta_k t}) dk, \quad (16)$$

where $\Delta_k = E_-(k) - \Delta_q$. Similar to Eq. (16), the interaction operator with channel B can also be written in an integral form. We consider the spontaneous decay process with an excitation initially localized in the emitter. In the single-excitation subspace, the state of the whole system is expressed as $|\psi(t)\rangle =$

$\sum_k [c_{ka}(t)|g, 1_{ka}\rangle + c_{kb}(t)|g, 1_{kb}\rangle] + c_e(t)|e, 0\rangle$, and the evolution of the whole system governed by H_{int} is derived from the following differential equations

$$\dot{c}_e(t) = -i \sum_k \frac{g e^{-i\Delta_k t}}{\sqrt{N}} \left[\cos^2 \frac{\theta_k}{2} c_{ka}(t) + \frac{\sin \theta_k}{2} c_{kb}(t) \right], \quad (17)$$

$$\dot{c}_{ka}(t) = -i \frac{g^*}{\sqrt{N}} e^{i\Delta_k t} \cos^2 \frac{\theta_k}{2} c_e(t), \quad (18)$$

$$\dot{c}_{kb}(t) = -i \frac{g^*}{\sqrt{N}} e^{i\Delta_k t} \frac{\sin \theta_k}{2} c_e(t). \quad (19)$$

By substituting the internal form of Eqs. (18, 19) into Eq. (17), the evolution of $c_e(t)$ is derived as

$$\dot{c}_e(t) = -\frac{g^2}{2\pi} \sum_{\pm} \left[\left(\frac{\cos \theta_{\pm k_r} + 1}{2} \right)^2 + \left(\frac{\sin \theta_{\pm k_r}}{2} \right)^2 \right] \left| \int_0^{\pm\pi} dk \int_0^t [c_e(t') e^{-i\Delta_k(t-t')}] dt' \right|. \quad (20)$$

As depicted in Fig. 2(a), we approximate the dispersion relation around $\pm k_r$ to be linear, i.e.,

$$v_g = \left. \frac{dE_-(k)}{dk} \right|_{k_r} = -2t \sin(k_r) \left(-\cos \phi + \frac{\sin^2 \phi \cos k_r}{\sqrt{f^2(k_r) + \eta^2}} \right), \quad (21)$$

where v_g is the group velocity at k_r ($k_r > 0$). By setting $\delta k = k - k_r$, the detuning is written as $\Delta_k \simeq v_g \delta k$. In the Born-Markovian regime, the decay rate is required to be much smaller than the band width $\{\delta_{+k_0}, \delta_{-k_0}\}$, and we can extend the integral bound $\pm\pi$ to be infinite. Consequently, Eq. (20) is reduced as

$$\dot{c}_e(t) = - \sum_{i=A,B} (\Gamma_{i+} + \Gamma_{i-}) c_e(t), \quad (22)$$

where $\Gamma_{i\pm}$ correspond to the emission rates into the right/left direction of channel i , which are derived as

$$\Gamma_{A\pm} = \frac{g^2}{2v_g} \left(\frac{\cos \theta_{\pm k_r} + 1}{2} \right)^2, \quad (23)$$

$$\Gamma_{B\pm} = \frac{g^2}{2v_g} \left(\frac{\sin \theta_{\pm k_r}}{2} \right)^2, \quad (24)$$

which show that $\Gamma_{A(B)\pm}$ are determined by $\theta_{\pm k_r}$. In this part we only focus on the Markovian decay regime (cyan area in Fig. 2) where both band edges and the upper energy band do not take apparent effects. We plot $\Gamma_{A,B}$ in Fig. 2(b) [in units of $g^2/(2v_g)$], and find that the emission to channel A (B) is spatially asymmetric (symmetric), i.e.,

$$\Gamma_{A+} > \Gamma_{A-}, \quad \Gamma_{B+} = \Gamma_{B-}.$$

Specially, under the following condition

$$\left(\frac{\cos \theta_{k_r} + 1}{2} \right)^2 \gg \left\{ \left(\frac{\cos \theta_{-k_r} + 1}{2} \right)^2, \left(\frac{\sin \theta_{\pm k_r}}{2} \right)^2 \right\}, \quad (25)$$

the emission field mostly distributes on the right side of channel A. Therefore, the spontaneous emission field will chirally propagate along the Hofstadter-ladder waveguide. As discussed in Sec. II, the chirality is led by the effective spin-orbit coupling mechanism.

We assume that the coupling position is at $x = 0$, and therefore, the field intensities on the right (left) side of channel A and B are defined as

$$\Phi_{A(B)\pm} = \sum_{x=0}^{\pm N/2} |c_{A(B),x}|^2, \quad (26)$$

where $c_{A(B),x}$ is the field amplitude of site $a(b)$ of the rung at x of the ladder. For example, if the right side of channel A is the desired direction, both the dissipation into channel B and into the left hand side of channel A will lead to photonic leakage. Consequently, the chiral factor \mathcal{C} is defined as [14]

$$\mathcal{C} = \frac{\Phi_{A+}}{\sum_{i=A,B} (\Phi_{i+} + \Phi_{i-})} = \frac{\Gamma_{A+}}{\sum_{i=A,B} (\Gamma_{i+} + \Gamma_{i-})}. \quad (27)$$

By adopting expressions of $\Gamma_{A(B)\pm}$ in Eqs. (23,24), the analytical chiral factor is derived as

$$\mathcal{C} = \frac{(f(k_r) + |f(k_r)|)^2}{(f(k_r) + |f(k_r)|)^2 + 2\eta^2}, \quad (28)$$

where we employ the relation $\tan \theta_k = \eta/f(k)$. In Fig. 2(b), we plot chiral factor \mathcal{C} changing with resonant

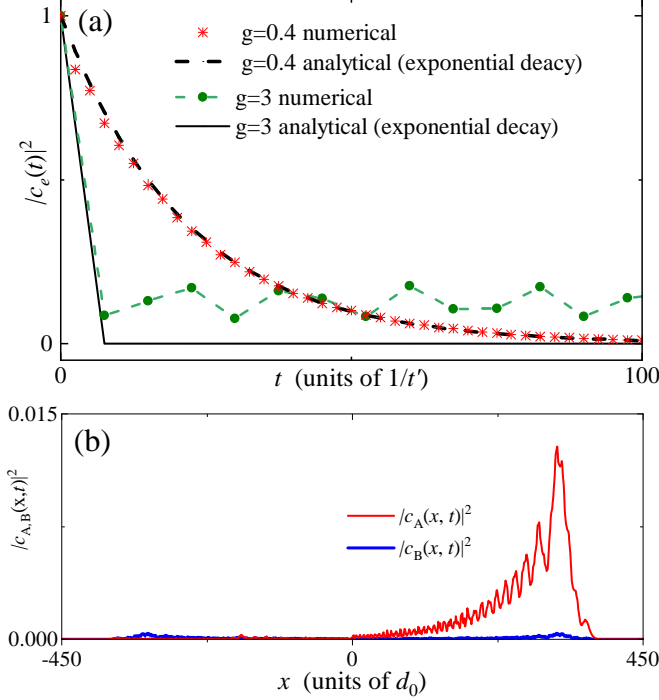


FIG. 3. (a) The spontaneous decay of the emitter by setting $g = 0.4$ and $g = 3$, respectively. The curves with (without) symbols correspond to numerical calculations (Markovian exponential decay). (b) Given that $g = 0.4$, the field distributions along channel A and B at $t = 100$. The parameters are adopted the same with those in Fig. 2.

wave number k_r . Given that $-\pi < \phi < 0$, $f(k_r) = \sin \phi \sin k_r < 0$ (Note that we have restricted k_r as positive, i.e., $k_r > 0$). In this case, $\mathcal{C} = 0$, indicating that the field hardly dissipates into the desired channel. When $0 < \phi < \pi$, the chiral factor is simplified as

$$\mathcal{C} = \frac{2f^2(k_r)}{2f^2(k_r) + \eta^2} = \frac{1}{1 + \frac{\eta^2}{2f^2(k_r)}}. \quad (29)$$

Therefore, under the condition

$$\frac{\eta^2}{2f^2(k_r)} \ll 1 \rightarrow \mathcal{C} \rightarrow 1, \quad (30)$$

most excitation energy will dissipate into the right side of channel A. Those discussions indicate that both the waveguide's parameters and the resonant position k_r will directly determine the chiral factor.

By adopting the parameters in Fig. 2, we obtain

$$\eta^2/[2f^2(k_r)] \simeq 0.058 \rightarrow \mathcal{C} \simeq 0.944, \quad (31)$$

which is a high chiral factor to realize cascaded quantum networks with multiple nodes. To verify our above analysis, in the following we numerically simulate the system's evolution by adopting the system's Hamiltonian in Eq. (9). Note that the ladder's Hamiltonian is

expressed in real space [see Eq. (1)], and the ladder length is set as $N = 1000$, which is long enough to avoid field reflection by the bounds. Figure 3(a) shows the evolution of the emitter with $g = 0.4$ and $g = 3$, respectively. Given that $g = 0.4$, the analytical decay rate is calculated as $\sum_{i=A,B} (\Gamma_{i+} + \Gamma_{i-}) \simeq 0.0014$ [according to Eqs. (23, 24)], which is much smaller than the band width $\delta_{\pm k_0}$, and the Markovian approximation is valid. The emitter's evolution $|c_e(t)|^2$ is shown in Fig. 3(a), which decays with time and matches well with the analytical exponential form. In Fig. 3(b), we plot the field distributions at $t = 100$ for both channel A and B, where the photonic field mostly distributes on the right side of channel A. By adopting Eq. (26) the numerical chirality is about $\mathcal{C} \simeq 0.943$, which is very close to the analytical result derived in Eq. (31).

Note that all the above results for the chiral decay are derived within the Born-Markovian approximation. When the emitter-waveguide interaction strength is comparable to the band width $\{\delta_{+k_0}, \delta_{-k_0}\}$, both modes around $k = 0$ and two energy minima points $k_{\pm \min}$ (see Fig. 2 and Fig. 5) with zero group velocity will prevent the emitter from decaying. Partial excitation energy will be trapped around the coupling position in the form of bound states [27]. By increasing the emitter-waveguide interaction beyond the Markovian regime with $g = 3$, we plot the emitter's evolution in Fig. 3(a), which is no longer of exponential decaying form. After dissipating partial energy into the waveguide, the rest is trapped within the emitter. Therefore, to work as a well-performed cascaded quantum system, the emitter in each node should couple to the waveguide within the Markovian regime. Next, we will discuss the behavior of bound states of both small and giant emitters due to band edge effects.

As discussed in experimental work in Refs. [81, 82], the bosonic modes in the Hofstadter-ladder waveguide can be made by cavities or LC resonators, which will experience decoherence led by the noisy environment. The decay of each site is assumed in the Lindblad form, i.e.,

$$\mathcal{L}\rho = \kappa \sum_{O=a,b} \sum_x O_x \rho O_x^\dagger - \frac{1}{2} (O_x^\dagger O_x \rho + \rho O_x^\dagger O_x), \quad (32)$$

where κ is the photonic decay rate of each cite. By setting $\kappa = 0$ and 0.01 respectively, we plot the corresponding field distributions along the waveguide at $t = 100$. When the photonic wavepacket propagates along the dissipative waveguide, it will decay the energy into the environment. We find that the amplitude of the photonic field becomes much lower than the non-dissipative case. However, the field distribution is still chiral, which is not affected by this local coherence.

Additionally, in experiments the waveguide's length cannot be infinite, and therefore, the chiral field will be reflected by the hard-wall boundary of the waveguide after a long-time propagation. In Fig. 4(c), we plot the field distribution at $t = 180$, when the wavepacket

already touches the waveguide's boundary. The energy flow direction is shown in the insets. We find that, due to the hopping rates t' between two channels at the boundary, most of the energy will be reflected into channel B. Since the photon decay of each rate is also considered, the amplitude of the reflected wavepacket is much lower than that in Fig. 4(a).

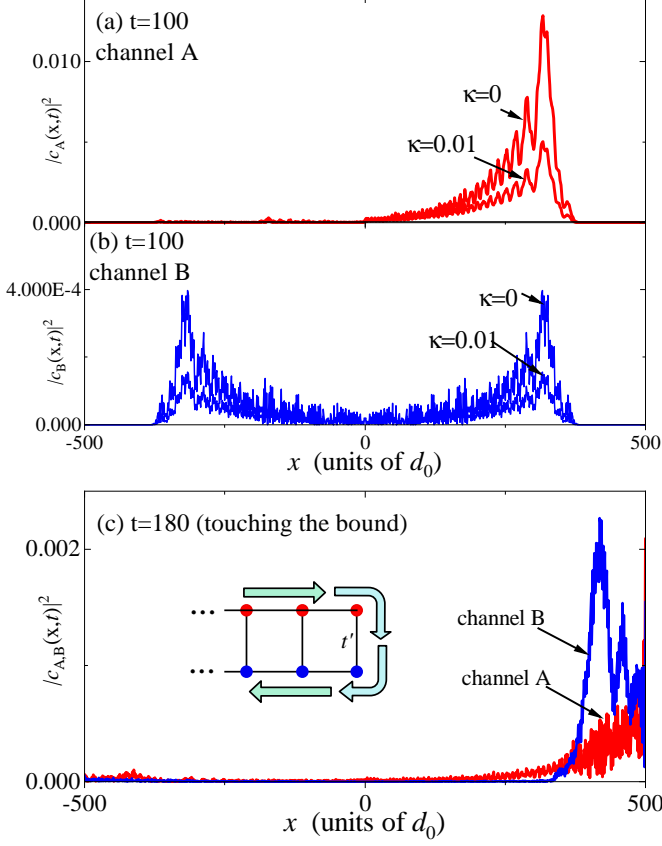


FIG. 4. (a, b) By setting the photonic decay rate for each site as $\kappa = 0$ and $\kappa = 0.01$, the field distributions along channel A and B at $t = 100$. (c) By setting $\kappa = 0.01$ the field distributions after being reflected by the hard-wall boundary of the waveguide. The energy flow direction is shown in the inset. Other parameters are adopted the same with those in Fig. 3.

IV. PERIODICAL INTERFERENCE BEHAVIOR MODULATED BY GIANT EMITTER'S SIZE

A. bound state of a single giant emitter

Besides emitting and absorbing real photons, different emitters can also be coherently mediated via exchanging virtual photons in the waveguide, which requires the emitter's frequency to be outside the spectrum of the waveguide bath [19, 22, 33]. Here we restrict the frequency detuning Δ_q below the lower bound of $E_-(k)$

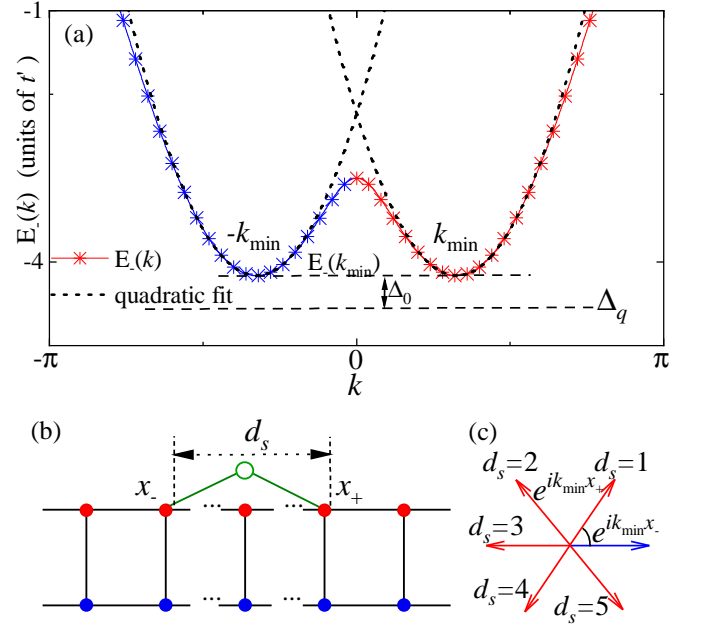


FIG. 5. (a) Around two energy minima $\pm k_{\min}$, the dispersion relation of the lower band can be fit with the quadratic relation [dashed curves, see Eq. (47)]. To observe bound states, the emitter's frequency is set below the band edge, i.e., $\Delta_q < E_{k_{\min}}$. (b) A giant emitter interacts with the waveguide at two coupling points x_{\pm} . The emitter's size is $d_s = x_+ - x_-$. (c) Given that $k_{\min} \simeq \pi/3$, the coupling phase relation between two coupling points changes with d_s .

[see Fig. 5(a)]. Additionally, the emitter is assumed to be of giant atom form [68–77], which couples to the waveguide at two points x_{\pm} of channel A (or B), as depicted in Fig. 5(b). The separation distance is denoted as $d_s = x_+ - x_-$, which corresponds to the giant emitter's size. Similar to previous discussions, the interaction strengths with channel A and B [see Eqs. (14,15)] are written as

$$g_{ka} = \frac{g}{\sqrt{N}} \cos^2 \frac{\theta_k}{2} (e^{-ikx_-} + e^{-ikx_+}), \quad (33)$$

$$g_{kb} = \frac{g}{\sqrt{N}} \cos \frac{\theta_k}{2} \sin \frac{\theta_k}{2} (e^{-ikx_-} + e^{-ikx_+}), \quad (34)$$

where g is the interaction strength with a single point. Note that under the condition $d_s = 0$, two coupling positions coincide at the same site, and the giant atom degrades as a small atom.

Similar to Eqs. (17–19), we can obtain differential equations for $c_e(t)$ and $c_{ka(b)}(t)$. Defining $e^{i\Delta_k t} \tilde{C}_{ka(b)}(t) = c_{ka(b)}(t)$, the evolution is derived in Laplace space with $c_e(t) \rightarrow \tilde{c}_e(s)$ and $C_{ka(b)}(t) \rightarrow \tilde{C}_{ka(b)}(s)$ [27, 33, 83]

$$s\tilde{c}_e(s) = -i \sum_k \left[g_{ka} \tilde{C}_{ka}(s) + g_{kb} \tilde{C}_{kb}(s) \right], \quad (35)$$

$$s\tilde{C}_{ki}(s) = -i\Delta_k \tilde{C}_{ki}(s) - ig_{ki}^* \tilde{c}_e(s), \quad i = a, b. \quad (36)$$

Consequently, $\tilde{C}_{ki}(s)$ is obtained as

$$\tilde{C}_{ki}(s) = \frac{-ig_{ki}^* c_e(s)}{s + i\Delta_k}, \quad i = a, b. \quad (37)$$

By substituting Eq. (37) into Eq. (35), $\tilde{c}_e(s)$ is derived as

$$\tilde{c}_e(s) = \frac{1}{s + \Sigma_e(s)}, \quad (38)$$

$$\Sigma_e(s) = \sum_k \frac{|g_{ka}|^2 + |g_{kb}|^2}{s + i\Delta_k}, \quad (39)$$

where $\Sigma_e(s)$ is the self-energy. The time-dependent evolution is recovered from the inverse Laplace transform [26]

$$c_e(t) = \frac{1}{2\pi i} \lim_{E \rightarrow \infty} \int_{\epsilon - iE}^{\epsilon + iE} \tilde{c}_e(s) e^{st} ds, \quad \epsilon > 0. \quad (40)$$

Given that the waveguide is long enough to avoid reflection effects, we can write the self-energy in the integral form by replacing Σ_k with $N/(2\pi) \int dk$. Substituting the relations

$$\cos^2 \frac{\theta_k}{2} = \frac{\frac{f(k)}{\sqrt{f^2(k) + \eta^2}} + 1}{2}, \quad (41)$$

$$\frac{\sin \theta_k}{2} = \frac{\frac{\eta}{\sqrt{f^2(k) + \eta^2}}}{2}, \quad (42)$$

into Eq. (39), the self-energy is expressed as

$$\Sigma_e(s) = \frac{1}{4\pi} \int_{-\pi}^{\pi} \frac{\left(\frac{f(k)}{\sqrt{f^2(k) + \eta^2}} + 1 \right) |G_k|^2}{s + i\Delta_k} dk, \quad (43)$$

where $G_k = g(e^{-ikx_-} + e^{-ikx_+})$.

Due to the effective spin-orbit coupling, the energy minimum point is split into two with non-zero momentum $\pm k_{\min} \neq 0$. At the positions of two dips, the group velocities are zero, which can be derived from Eq. (21)

$$v_g = \left. \frac{dE_-(k)}{dk} \right|_{k=\pm k_{\min}} = 0. \quad (44)$$

Therefore, their positions are derived as

$$\sin(k_{\min}) = \pm \sqrt{\sin^2 \phi - \eta^2 \cot^2 \phi}. \quad (45)$$

At $\pm k_{\min}$, the second-order derivatives are non-zero, and we denote the curvature as

$$\alpha = \left. \frac{d^2 E_-(k)}{dk^2} \right|_{k=\pm k_{\min}}. \quad (46)$$

As depicted in Fig. 5(a), we employ the effective mass approximation, to fit the dispersion around the band edges with quadratic relations

$$E_-(k) = E_{\min} + \alpha (k \pm k_{\min})^2. \quad (47)$$

By substituting Eq. (47) into Eq. (43), the self-energy is calculated as

$$\Sigma_e(s) \simeq \frac{1}{4\pi} \left\{ \int_{-\pi}^0 \frac{\left(\frac{f(k)}{\sqrt{f^2(k) + \eta^2}} + 1 \right) |G_k|^2}{s + i \left[\Delta_0 + \alpha (k + k_{\min})^2 \right]} dk + \int_0^{\pi} \frac{\left(\frac{f(k)}{\sqrt{f^2(k) + \eta^2}} + 1 \right) |G_k|^2}{s + i \left[\Delta_0 + \alpha (k - k_{\min})^2 \right]} dk \right\}, \quad (48)$$

where $\Delta_0 = E_{\min} - \Delta_g$ is the detuning to the band edge [see Fig. 5(a)]. We assume that Δ_0 is small, and therefore, only the modes around $\pm k_{\min}$ contribute significantly to $\Sigma_e(s)$. Consequently, we can approximate

$$G_{\pm k} \simeq G_{\pm k_{\min}}, \quad f(\pm k) \simeq f(\pm k_{\min}), \quad (49)$$

and extend the integral bound of Eq. (48) to be infinite. Finally, we obtain

$$\Sigma_e(s) \simeq \frac{|G_{k_{\min}}|^2}{2} \frac{1}{\sqrt{-\alpha (\Delta_0 - is)}}, \quad (50)$$

where we have employed the following relations

$$|G_{k_{\min}}| = |G_{-k_{\min}}|, \quad f(k_{\min}) = -f(-k_{\min}). \quad (51)$$

In this work, the adopted parameters of the waveguide satisfy

$$\sin^2 \phi \gg \eta^2 \cot^2 \phi \longrightarrow k_{\min} \simeq \phi = \pi/3. \quad (52)$$

As shown in Fig. 5(c), the phase relation between two coupling points will rotate counter-clockwise when increasing giant emitter's size ($d_s = 0, 1, 2, 3, \dots$). Therefore, the relative phase between x_{\pm} is very essential for the dynamics of the giant emitter. The interference between two points is maximum destructive (constructive) given that $d_s = 3(2N + 1)$ ($d_s = 6N$). When Δ_0 is much stronger than $G_{k_{\min}}$, most energy will be trapped in the emitter in the form of the bound state [27, 31, 83]. The trapped excitation probability is determined by the pure imaginary pole s_0 of the following transcendental equation [83]

$$s_0 + \Sigma_e(s_0) \simeq s_0 + \frac{|G_{k_{\min}}|^2}{2} \frac{1}{\sqrt{-\alpha (\Delta_0 - is_0)}} = 0, \quad (53)$$

and the steady state population of the emitter is derived via the residue theorem [27]

$$|c_e(t = \infty)|^2 = |\text{Res}(s_0)|^2, \quad (54)$$

$$\text{Res}(s_0) = \left. \frac{1}{1 + \partial_s \Sigma_e(s)} \right|_{s=s_0}. \quad (55)$$

In Fig. 6(a), we plot dynamical evolutions of $|c_e(t)|^2$ for different giant emitter's sizes d_s . When $d_s = 0$ (a

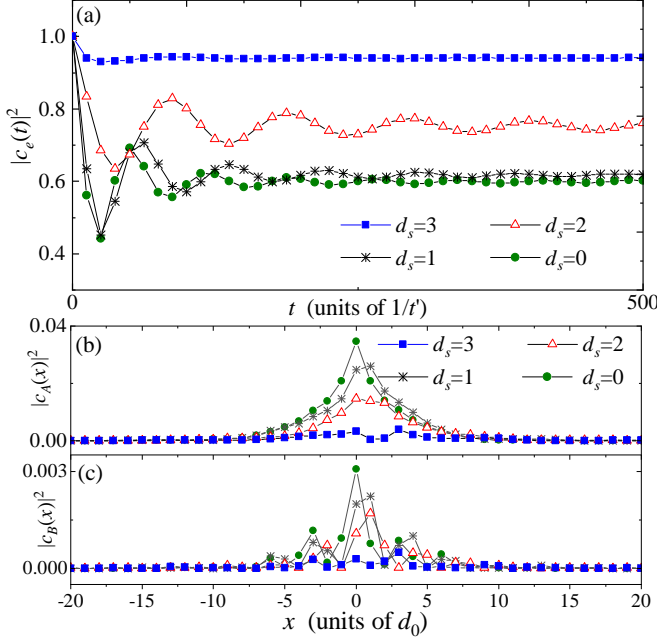


FIG. 6. (a) The probabilities $|c_e(t)|^2$ of the giant emitter remaining in its excited state change with t for different d_s . In the limit $t \rightarrow \infty$, $|c_e(t)|^2$ reaches its steady value, which is nonzero due to the band edge effect. The corresponding field distributions of the photonic bound states in channel A and B are shown in (b) and (c), respectively. The emitter frequency is set below the lower band with $\Delta_q = -4.2$. The coupling strength is $g = 0.1$. The waveguide parameters are the same with those in Fig. 2.

small emitter), the effective interacting strength $|G_{k_{\min}}|$ is strongest, which is enhanced by the constructive interference between two coupling legs. The steady state $|c_e(t)|^2$ reaches lowest, and the emitter can effectively distribute its energy into the waveguide. That is, the photonic bound state is mostly localized in channel A due to the relation

$$\cos^2 \frac{\theta_{k_{\min}}}{2} \gg \cos \frac{\theta_{k_{\min}}}{2} \sin \frac{\theta_{k_{\min}}}{2}, \quad (56)$$

which can be seen clearly by comparing Fig. 6(b) and Fig. 6(c).

When increasing the distance between two coupling points, the constructive interference will be reversed as destructive, with $|G_{k_{\min}}|$ being significantly weakened. When $d_s = 3$, the phase difference satisfies $k_{\min}d_s \simeq \pi$, indicating that the interaction strength is approximately zero, i.e., $|G_{k_{\min}}| \simeq 0$ [see Fig. 5(c)]. The giant emitter approximately decouples with the waveguide. Due to this decoupling mechanism, the excitation trapped in the emitter reaches its maximum, as shown in Fig. 6(a). Figure 6(b, c) show that the destructive interference will also suppress the bound state's amplitude significantly. We plot the steady state population $|c_e(t \rightarrow \infty)|^2$ changing with d_s in Fig. 7(a), which clearly presents a periodical interference pattern of $|c_e(t \rightarrow \infty)|^2$

modulated by the giant atom's size. Note that we only take $k_{\min} \simeq \pi/3$ for example. Note that The periodical length is tunable by controlling the parameters of the Hofstadter ladder waveguide. By adopting another k_{\min} according Eq. (45), different spatial interference patterns can also be observed. The oscillating pattern in Fig. 7(a) is due to interference between different points in the giant atom, and the peaks (dips) correspond to the positions where the maximum constructive (destructive) interference happens. Therefore, we can define the contrast ratio R for the interference as

$$R = \frac{\min\{|c_e(t \rightarrow \infty, d_s)|^2\}}{\max\{|c_e(t \rightarrow \infty, d_s)|^2\}}. \quad (57)$$

For the parameters employed in Fig. 7(a), $\min\{|c_e(t \rightarrow \infty, d_s)|^2\}$ ($\max\{|c_e(t \rightarrow \infty, d_s)|^2\}$) is located at $d_s = 0$ ($d_s = \pm 3$), which corresponds to a small (giant) atom. A smaller R indicates that the dynamical difference between small and giant atoms is more apparent. In Fig. 7(b), we plot maximum/minimum $|c_e(t \rightarrow \infty, d_s)|^2$ and R changing with the frequency detuning Δ_q . When shifting Δ_q away from the band edge, the contributions of the band-edge modes to the bound states will be significantly suppressed. Therefore, a larger Δ_q will reduce the interference effects, which corresponds to $R \rightarrow 1$ [see Fig. 7(b)]. To observe better interference effect in experiments, the emitter frequency can be close to the edge of the lower energy band.

B. dipole-dipole interactions

By exchanging virtual photons in the waveguide, between emitters there are long-range dipole-dipole interactions which are determined by the overlap areas between their bound states [18, 19, 33]. As shown in Fig. 8(a, b), we now discuss the multiple emitters interacting with the same ladder waveguide. Due to the interference mechanism presented above, we focus on revealing the relation between giant emitter's size and the quantum dynamics where dipole-dipole interactions are involved.

Both two giant emitters are assumed to couple with channel A, and the coupling topology is of separation form [70]. Similar to the single emitter case, the interaction Hamiltonian is written as

$$H_{\text{int},2} = \sum_{i=1,2} \sum_k \frac{G_{ik}}{\sqrt{N}} \cos \frac{\theta_k}{2} \sigma_i^- C_{k-}^\dagger + \text{H.c.}, \quad (58)$$

where $G_{ik} = g(e^{-ikx_i^-} + e^{-ikx_i^+})$ is the coupling strength between emitter i and the waveguide. We consider two emitters with identical frequency Δ_q which is also below the lower bound of $E_-(k)$. To proceed, we define the average distance between two emitters as

$$D_q = \frac{x_+^2 + x_-^2}{2} - \frac{x_+^1 + x_-^1}{2}. \quad (59)$$

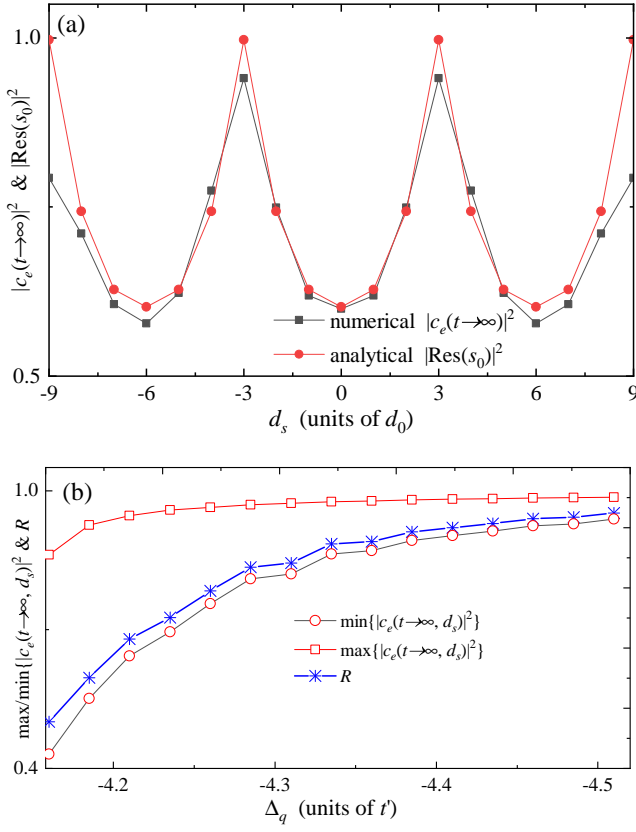


FIG. 7. (a) The periodical behavior of the trapped excitation $|c_e(t \rightarrow \infty)|^2$ changing with the size of giant emitters. The analytical results are calculated via the residue theorem in Eq. (55). (b) The maximum/minimum $|c_e(t \rightarrow \infty, d_s)|^2$ and the contrast ratio R changes with the emitter frequency Δ_q .

The dipole-dipole interaction can be tediously derived via the standard resolvent-operator techniques [18, 19, 22, 33]. However, given that the detuning Δ_0 is large and the waveguide is only virtually excited, J_0 corresponds to the effective coupling strength mediated by the waveguide's modes, which can be simply derived via the effective Hamiltonian methods [84]. In the rotating frame of free energies of both emitters and waveguide, we first write $H_{\text{int},2}$ in Eq. (58) in the time-dependent form

$$H_{\text{int},2}(t) = \sum_{i=1,2} \sum_k \frac{G_{ik}}{\sqrt{N}} \cos \frac{\theta_k}{2} e^{i\Delta_k t} \sigma_i^- C_{k-}^\dagger + \text{H.c.}, \quad (60)$$

where $\Delta_k = E_-(k) - \Delta_q$. We first calculate the coupling rate $J_{12,k}$ mediated by one mode k . By employing the methods in Ref. [76], the one-mode-mediated effective Hamiltonian is derived as

$$H_{q-q,k} = \frac{G_{1k} G_{2k}^* \cos^2 \frac{\theta_k}{2}}{\Delta_k N} \times (\sigma_1^- C_{k-}^\dagger \sigma_2^+ C_{k-} - \sigma_2^+ C_{k-} \sigma_1^- C_{k-}^\dagger) + \text{H.c.} \quad (61)$$

Since the waveguide is only virtually excited and

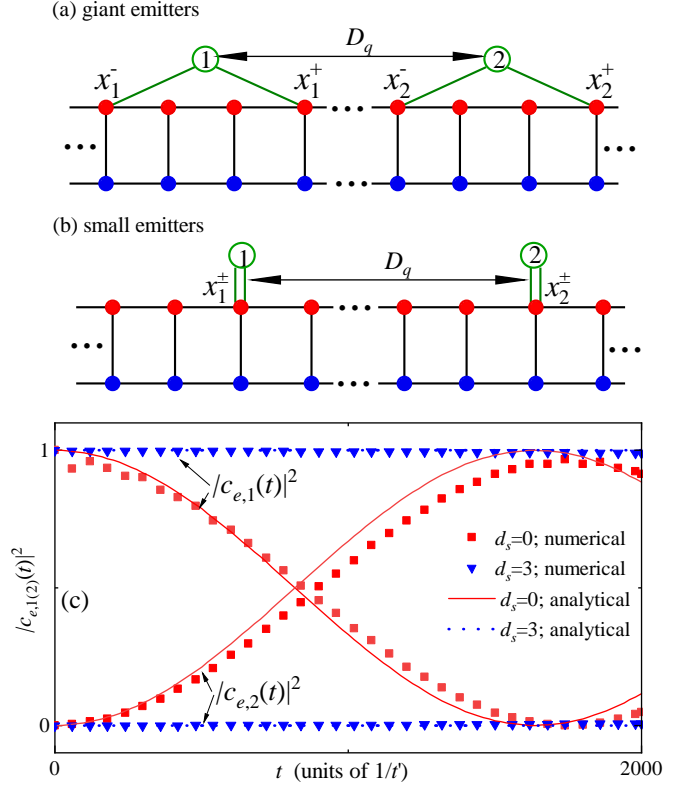


FIG. 8. (a) Two giant and (b) two small emitters, which are separated with distance D_q , interact with a common ladder waveguide. For giant emitter i , the coupling points are located at different positions x_i^\pm . For small emitter i , x_i^\pm are coincided at the same site. (c) The Rabi oscillations between two giant (small) emitters which are marked with triangles (squares). The corresponding analytical results (curves without symbols) are derived from Eq. (68). The separation distances between two emitters in (a, b) are set as $D_q = 4$. To avoid virtual photons in the waveguide being excited with high probabilities, we adopt a weak coupling strength $g = 0.015$. The other parameters are the same with those in Fig. 6.

approximately in its vacuum state, we can trace off the freedom of mode k by adopting the following approximation

$$\langle C_{k-}^\dagger C_{k-} \rangle \simeq 0, \quad \langle C_{k-} C_{k-}^\dagger \rangle \simeq 1. \quad (62)$$

Consequently, $H_{q-q,k}$ is simplified as

$$H_{q-q,k} \simeq -\frac{G_{1k} G_{2k}^* \cos^2 \frac{\theta_k}{2}}{\Delta_k N} \sigma_2^+ \sigma_1^- + \text{H.c.} \quad (63)$$

Note that $H_{q-q,k}$ is mediated by one mode, and the total dipole-dipole interaction should take all the modes' contribution into account. Consequently, the total dipole-dipole interaction Hamiltonian mediated by all the waveguide's modes is derived as

$$H_{q-q} = \sum_k H_{q-q,k} = J_{12} (\sigma_1^- \sigma_2^+ + \text{H.c.}). \quad (64)$$

where J_{12} is the total interaction strength which is written as

$$J_{12} = - \sum_k \frac{G_{1k} G_{2k}^* \cos^2 \frac{\theta_k}{2}}{\Delta_k N} \simeq - \frac{1}{2\pi} \int_{-\pi}^{\pi} \frac{G_{1k} G_{2k}^* \cos^2 \frac{\theta_k}{2}}{\Delta_k} dk. \quad (65)$$

Since the emitter frequency is below the edge of the lower energy band [see Fig. 5(a)], the dispersion relation can be fit with the quadratic relations in Eq. (47). Without loss of generality, we set $(x_+^1 + x_-^1)/2 = 0$ since only relative distance matters. As depicted in Fig. 8(a), two emitters are separated with a distance D_q . Given that $D_q > d_s$, J_{12} can be written as

$$J_{12} \simeq - \frac{1}{2\pi} \left\{ \int_{-\pi}^0 \frac{|G_{1k}| |G_{2k}^*| e^{ikD_q} \left(\frac{\cos \theta_k + 1}{2} \right)}{\Delta_0 + \alpha(k + k_{\min})^2} dk + \int_0^{\pi} \frac{|G_{1k}| |G_{2k}^*| e^{ikD_q} \left(\frac{\cos \theta_k + 1}{2} \right)}{\Delta_0 + \alpha(k - k_{\min})^2} dk \right\} \quad (66)$$

As shown in Eq. (23) and depicted in Fig. 2(b), the following relation

$$\left| \frac{\cos \theta_{-k} + 1}{2} \right| \ll \left| \frac{\cos \theta_k + 1}{2} \right| \simeq 1, \quad k > 0$$

is valid for the parameters employed in this work. Consequently, we can neglect the first part ($k < 0$) in Eq. (66), and J_{12} is derived as

$$J_{12} \simeq \int_0^{\pi} \frac{|G_{1k}| |G_{2k}^*| e^{ikD_q}}{\Delta_0 + \alpha(k - k_{\min})^2} dk, \quad (67)$$

which indicates that that dipole-dipole interactions are determined by the overlap areas between two bound states of emitters [18]. Similar to the process obtaining the self-energy in Eqs. (48, 50), we derive J_{12} as

$$J_{12} = \frac{|G_{1k_{\min}}| |G_{2k_{\min}}^*|}{2\sqrt{\alpha\Delta_0}} e^{-|\sqrt{\frac{\Delta_0}{\alpha}} D_q|}, \quad (68)$$

which shows that J_{12} exponentially decays with emitters' separation distance. Similar results have been obtained in Refs. [18, 19, 22].

As shown in Fig. 7(b, c), the amplitude of the bound state will periodically change with d_s due to the interference effect. When $d_s = 3$, the photonic bound state approximately disappears. Consequently, the overlapping area is also nearly zero. By assuming the initial excitation being in emitter 1, we numerically plot the Rabi oscillations between giant emitters ($d_s = 3$) and small emitters ($d_s = 0$) in Fig. 8(c), respectively. We find that, due to the destructive interference, when $d_s = 3$, two emitters hardly exchange energy, and decouple with each other ($J_{12} \simeq 0$). On the contrary, two emitters will

exchange excitation rapidly at a large rate due to the constructive interference when d_s is reduced to be zero.

V. CONCLUSION AND OUTLOOKS

In this work, we explore the unconventional quantum optics by considering a Hofstadter-ladder waveguide interacting with both small and giant emitters. Due to the effective spin-orbit coupling, both the waveguide's vacuum modes and spectrum show nontrivial properties. In the first part, we consider a small emitter which frequency is resonant with one energy band. Two legs of the ladder, which can be viewed as the freedoms in an effective spin locked with the momentum freedom, provide two dissipating channels. The spontaneous emission is chiral with most photonic field decaying unidirectionally. Both numerical and analytical results show that the Hofstadter-ladder waveguide can work as a well-performed quantum bus of a chiral network.

In the second part, the emitters are assumed of giant atom form with frequencies below the lower energy band. In this scenario, only the modes around two energy minima points induced by the spin-orbit coupling contribute significantly to the system's dynamics, which will lead to emitter-waveguide bound states. Since the energy minima modes carry non-zero momentum, the coupling strengths are periodically modulated by the giant emitter's size due to quantum interference. Specially the giant emitter will decouple with the waveguide when maximum destructive interference happens. This mechanism provides a novel approach to control long-range dipole-dipole interactions between emitters by modulating their sizes.

In this work, the giant emitter is assumed to couple with the sites of the same channel. Other intriguing effects might be observed by considering the coupling points on different channels. Moreover, for multiple giant emitters, we just consider the coupling points arranged in the separation form. In fact there are some other distinct topologies, which are nested and braided cases [70]. Exploring the coupling topology effects might also bring novel quantum phenomena. There are already plenty of work about realizing artificial Hofstadter ladders in various quantum systems such as cold atoms and circuit-QED [54, 56, 85, 86], which can be potential platforms to demonstrate above unconventional QED phenomena. We hope that our work will open the possibilities of exploring novel quantum effects in artificial spin-orbit-coupling environments.

VI. ACKNOWLEDGMENTS

The quantum dynamical simulations are based on open source code QuTiP [87, 88]. X.W. is supported by the National Natural Science Foundation of China (NSFC) (Grant No. 12174303 and No. 11804270), and China Postdoctoral Science Foundation No. 2018M631136. H.R.L. is supported by the National Natural Science Foundation of China (NSFC) (Grant No.11774284).

-
- [1] C. Cohen-Tannoudji, J. Dupont-Roc, and G. Grynberg, *Atom-Photon Interactions* (Wiley, 1998).
- [2] A. A. Clerk, M. H. Devoret, S. M. Girvin, F. Marquardt, and R. J. Schoelkopf, "Introduction to quantum noise, measurement, and amplification," *Rev. Mod. Phys.* **82**, 1155 (2010).
- [3] W. E. Lamb and R. C. Retherford, "Fine structure of the hydrogen atom by a microwave method," *Phys. Rev.* **72**, 241 (1947).
- [4] Marlan O. Scully and M. Suhail Zubairy, *Quantum Optics* (Cambridge University Press, 1997).
- [5] S. John and T. Quang, "Spontaneous emission near the edge of a photonic band gap," *Phys. Rev. A* **50**, 1764 (1994).
- [6] P. Lambropoulos, G. M. Nikolopoulos, T. R. Nielsen, and S. Bay, "Fundamental quantum optics in structured reservoirs," *Rep. Prog. Phys.* **63**, 455 (2000).
- [7] F. Giraldi and F. Petruccione, "Reservoir for inverse-power-law decoherence of a qubit," *Phys. Rev. A* **83**, 012107 (2011).
- [8] P. Lodahl, S. Mahmoodian, and S. Stobbe, "Interfacing single photons and single quantum dots with photonic nanostructures," *Rev. Mod. Phys.* **87**, 347 (2015).
- [9] M. Stewart, J. Kwon, A. Lanuza, and D. Schneble, "Dynamics of matter-wave quantum emitters in a structured vacuum," *Phys. Rev. Research* **2**, 043307 (2020).
- [10] V. S. Ferreira, J. Banker, A. Sipahigil, M. H. Matheny, A. J. Keller, E. Kim, M. Mirhosseini, and O. Painter, "Collapse and revival of an artificial atom coupled to a structured photonic reservoir," *Phys. Rev. X* **11**, 041043 (2021).
- [11] J. Petersen, J. Volz, and A. Rauschenbeutel, "Chiral nanophotonic waveguide interface based on spin-orbit interaction of light," *Science* **346**, 67 (2014).
- [12] K. Y. Bliokh and F. Nori, "Transverse and longitudinal angular momenta of light," *Phys. Rep.* **592**, 1 (2015).
- [13] K. Y. Bliokh, F. J. Rodríguez-Fortuño, F. Nori, and A. V. Zayats, "Spin-orbit interactions of light," *Nature Photon.* **9**, 796 (2015).
- [14] P. Lodahl, S. Mahmoodian, S. Stobbe, A. Rauschenbeutel, P. Schneeweiss, J. Volz, H. Pichler, and P. Zoller, "Chiral quantum optics," *Nature (London)* **541**, 473 (2017).
- [15] B. Lang, D. P. S. McCutcheon, E. Harbord, A. B. Young, and R. Oulton, "Perfect chirality with imperfect polarization," *Phys. Rev. Lett.* **128**, 073602 (2022).
- [16] S. John and J. Wang, "Quantum electrodynamics near a photonic band gap: Photon bound states and dressed atoms," *Phys. Rev. Lett.* **64**, 2418 (1990).
- [17] A. Goban, C.-L. Hung, S.-P. Yu, J.D. Hood, J.A. Muniz, J.H. Lee, M.J. Martin, A.C. McClung, K.S. Choi, D.E. Chang, O. Painter, and H.J. Kimble, "Atom-light interactions in photonic crystals," *Nat. Commun.* **5**, 4808 (2014).
- [18] A. González-Tudela, C.-L. Hung, D. E. Chang, J. I. Cirac, and H. J. Kimble, "Subwavelength vacuum lattices and atom-atom interactions in two-dimensional photonic crystals," *Nature Photon.* **9**, 320 (2015).
- [19] J. S. Douglas, T. Caneva, and D. E. Chang, "Photon molecules in atomic gases trapped near photonic crystal waveguides," *Phys. Rev. X* **6**, 031017 (2016).
- [20] Y. B. Liu and A. A. Houck, "Quantum electrodynamics near a photonic bandgap," *Nat. Phys.* **13**, 48 (2017).
- [21] D. E. Chang, J. S. Douglas, A. González-Tudela, C.-L. Hung, and H. J. Kimble, "Colloquium: Quantum matter built from nanoscopic lattices of atoms and photons," *Rev. Mod. Phys.* **90**, 031002 (2018).
- [22] X. Wang, T. Liu, A. F. Kockum, H.-R. Li, and F. Nori, "Tunable chiral bound states with giant atoms," *Phys. Rev. Lett.* **126**, 043602 (2021).
- [23] J. S. Douglas, H. Habibian, C.-L. Hung, A. V. Gorshkov, H. J. Kimble, and D. E. Chang, "Quantum many-body models with cold atoms coupled to photonic crystals," *Nature Photon.* **9**, 326 (2015).
- [24] E. Shahmoon and G. Kurizki, "Nonradiative interaction and entanglement between distant atoms," *Phys. Rev. A* **87**, 033831 (2013).
- [25] L. Ying, M. Zhou, M. Mattei, B.-Y. Liu, P. Campagnola, R. H. Goldsmith, and Z.-F. Yu, "Extended range of dipole-dipole interactions in periodically structured photonic media," *Phys. Rev. Lett.* **123**, 173901 (2019).
- [26] T. Ramos, B. Vermersch, P. Hauke, H. Pichler, and P. Zoller, "Non-markovian dynamics in chiral quantum networks with spins and photons," *Phys. Rev. A* **93**, 062104 (2016).
- [27] G. Calajo, F. Ciccarello, D. Chang, and P. Rabl, "Atom-field dressed states in slow-light waveguide QED," *Phys. Rev. A* **93**, 033833 (2016).
- [28] A. González-Tudela and J. I. Cirac, "Exotic quantum dynamics and purely long-range coherent interactions in dirac conelike baths," *Phys. Rev. A* **97**, 043831 (2018).
- [29] A. González-Tudela, C. S. Muñoz, and J. I. Cirac, "Engineering and harnessing giant atoms in high-dimensional baths: A proposal for implementation with cold atoms," *Phys. Rev. Lett.* **122**, 203603 (2019).
- [30] L. Leonforte, A. Carollo, and F. Ciccarello, "Vacancy-like dressed states in topological waveguide qed," *Phys. Rev. Lett.* **126**, 063601 (2021).
- [31] A. González-Tudela and J. I. Cirac, "Markovian and non-markovian dynamics of quantum emitters coupled to two-dimensional structured reservoirs," *Phys. Rev. A* **96**, 043811 (2017).
- [32] A. González-Tudela and J. I. Cirac, "Quantum emitters in two-dimensional structured reservoirs in the nonperturbative regime," *Phys. Rev. Lett.* **119**, 143602 (2017).
- [33] M. Bello, G. Platero, J. I. Cirac, and A. González-Tudela, "Unconventional quantum optics in topological waveguide QED," *Sci. Adv.* **5**, eaaw0297 (2019).
- [34] E. Kim, X. Zhang, V. S. Ferreira, J. Banker, J. K. Iverson, A. Sipahigil, M. Bello, A. González-Tudela, M. Mirhosseini, and O. Painter, "Quantum electrodynamics in a topological waveguide," *Phys. Rev. X* **11**, 011015 (2021).
- [35] F. Roccati, S. Lorenzo, G. Calajò, G. M. Palma, A. Carollo, and F. Ciccarello, "Exotic interactions mediated by a non-hermitian photonic bath," *Optica* **9**, 565–571 (2022).
- [36] Z. Gong, M. Bello, D. Malz, and F. K. Kunst, "Bound states and photon emission in non-hermitian nanophotonics," *preprint arXiv:2205.05490* (2022).

- [37] S.-F. Zhang, “Spin hall effect in the presence of spin diffusion,” *Phys. Rev. Lett.* **85** (2000), 10.1103/PHYS-REVLETT.85.393.
- [38] S. Murakami, N. Nagaosa, and S.-C. Zhang, “Dissipationless quantum spin current at room temperature,” *Science* **301**, 1348 (2003).
- [39] J. Sinova, D. Culcer, Q. Niu, N. A. Sinitsyn, T. Jungwirth, and A. H. MacDonald, “Universal intrinsic spin hall effect,” *Phys. Rev. Lett.* **92**, 126603 (2004).
- [40] J. Wunderlich, B. Kaestner, J. Sinova, and T. Jungwirth, “Experimental observation of the spin-hall effect in a two-dimensional spin-orbit coupled semiconductor system,” *Phys. Rev. Lett.* **94**, 047204 (2005).
- [41] C. L. Kane and E. J. Mele, “Quantum spin hall effect in graphene,” *Phys. Rev. Lett.* **95**, 226801 (2005).
- [42] V. Galitski and I. B. Spielman, “Spin-orbit coupling in quantum gases,” *Nature (London)* **494**, 49 (2013).
- [43] X.-F. Zhou, Y. Li, Z. Cai, and C.J. Wu, “Unconventional states of bosons with the synthetic spin-orbit coupling,” *J. Phys. B: At., Mol. Opt. Phys.* **46**, 134001 (2013).
- [44] Z. Wu, L. Zhang, W. Sun, X.-T. Xu, B.-Z. Wang, S.-C. Ji, Y.-J. Deng, S. Chen, X.-J. Liu, and J.-W. Pan, “Realization of two-dimensional spin-orbit coupling for bose-einstein condensates,” *Science* **354**, 83 (2016).
- [45] Y. V. Kartashov, V. V. Konotop, and L. Torner, “Bound states in the continuum in spin-orbit-coupled atomic systems,” *Phys. Rev. A* **96**, 033619 (2017).
- [46] L. F. Livi, G. Cappellini, M. Diem, L. Franchi, C. Clivati, M. Frittelli, F. Levi, D. Calonico, J. Catani, M. Inguscio, and L. Fallani, “Synthetic dimensions and spin-orbit coupling with an optical clock transition,” *Phys. Rev. Lett.* **117**, 220401 (2016).
- [47] L.-Q. Liu, T. Moriyama, D. C. Ralph, and R. A. Buhrman, “Spin-torque ferromagnetic resonance induced by the spin hall effect,” *Phys. Rev. Lett.* **106** (2011), 10.1103/PhysRevLett.106.036601.
- [48] V. G. Sala, D. D. Solnyshkov, I. Carusotto, T. Jacqmin, A. Lemaître, H. Terças, A. Nalitov, M. Abbarchi, E. Galopin, I. Sagnes, J. Bloch, G. Malpuech, and A. Amo, “Spin-orbit coupling for photons and polaritons in microstructures,” *Phys. Rev. X* **5**, 011034 (2015).
- [49] G. Salerno, A. Berardo, T. Ozawa, H. M. Price, L. Taxis, N. M. Pugno, and I. Carusotto, “Spin-orbit coupling in a hexagonal ring of pendula,” *New J. Phys.* **19**, 055001 (2017).
- [50] M. Creutz, “Aspects of chiral symmetry and the lattice,” *Rev. Mod. Phys.* **73**, 119 (2001).
- [51] B. N. Narozhny, S. T. Carr, and A. A. Nersisyan, “Fractional charge excitations in fermionic ladders,” *Phys. Rev. B* **71**, 161101 (2005).
- [52] A. Jaefari and E. Fradkin, “Pair-density-wave superconducting order in two-leg ladders,” *Phys. Rev. B* **85**, 035104 (2012).
- [53] M. Atala, M. Aidelsburger, M. Lohse, J. T. Barreiro, B. Paredes, and I. Bloch, “Observation of chiral currents with ultracold atoms in bosonic ladders,” *Nature Physics* **10**, 588 (2014).
- [54] M. E. Tai, A. Lukin, M. Rispoli, R. Schittko, T. Menke, D. Borgnia, P. M. Preiss, F. Grusdt, A. M. Kaufman, and M. Greiner, “Microscopy of the interacting Harper-hofstadter model in the two-body limit,” *Nature (London)* **546**, 519–523 (2017).
- [55] L.-Q. Yuan, Q. Lin, A.-W. Zhang, M. Xiao, X.-F. Chen, and S.H. Fan, “Photonic gauge potential in one cavity with synthetic frequency and orbital angular momentum dimensions,” *Phys. Rev. Lett.* **122**, 083903 (2019).
- [56] X. Guan, Y.-L. Feng, Z.-Y. Xue, G. Chen, and S.T. Jia, “Synthetic gauge field and chiral physics on two-leg superconducting circuits,” *Phys. Rev. A* **102**, 032610 (2020).
- [57] D. Hügél and B. Paredes, “Chiral ladders and the edges of quantum hall insulators,” *Phys. Rev. A* **89**, 023619 (2014).
- [58] E. Sánchez-Burillo, C. Wan, D. Zueco, and A. González-Tudela, “Chiral quantum optics in photonic sawtooth lattices,” *Phys. Rev. Research* **2**, 023003 (2020).
- [59] X. Wang, H.-R. Li, and F.-L. Li, “Generating synthetic magnetism via floquet engineering auxiliary qubits in phonon-cavity-based lattice,” *New J. Phys.* **22**, 033037 (2020).
- [60] D. De Bernardis, Z.-P. Cían, I. Carusotto, M. Hafezi, and P. Rabl, “Light-matter interactions in synthetic magnetic fields: Landau-photon polaritons,” *Phys. Rev. Lett.* **126**, 103603 (2021).
- [61] X.-L. Dong, P.-B. Li, T. Liu, and F. Nori, “Unconventional quantum sound-matter interactions in spin-optomechanical-crystal hybrid systems,” *Phys. Rev. Lett.* **126**, 203601 (2021).
- [62] S. Mittal, J. Fan, S. Faez, A. Migdall, J. M. Taylor, and M. Hafezi, “Topologically robust transport of photons in a synthetic gauge field,” *Phys. Rev. Lett.* **113**, 087403 (2014).
- [63] G. Calajó, M. J. A. Schuetz, H. Pichler, M. D. Lukin, P. Schneeweiss, J. Volz, and P. Rabl, “Quantum acousto-optic control of light-matter interactions in nanophotonic networks,” *Phys. Rev. A* **99**, 053852 (2019).
- [64] N. Gheeraert, S. Kono, and Y. Nakamura, “Programmable directional emitter and receiver of itinerant microwave photons in a waveguide,” *Phys. Rev. A* **102**, 053720 (2020).
- [65] X. Wang, Y.-F. Lin, J.-Q. Li, W.-X. Liu, and H.-R. Li, “Chiral SQUID-metamaterial waveguide for circuit-QED,” *preprint arXiv:2206.06579* (2022).
- [66] P. Solano, P. Barberis-Blostein, and K. Sinha, “Dissimilar collective decay and directional emission from two quantum emitters,” *preprint arXiv:2108.12951* (2021).
- [67] B. Kannan, A. Almanakly, Y. Sung, A. D. Paolo, D. A. Rower, J. Braumüller, A. Melville, B. M. Niedzielski, A. Karamlou, and K. Serniak, “On-demand directional photon emission using waveguide quantum electrodynamics,” *preprint arXiv:2203.01430* (2022).
- [68] A. F. Kockum, P. Delsing, and G. Johansson, “Designing frequency-dependent relaxation rates and Lamb shifts for a giant artificial atom,” *Phys. Rev. A* **90**, 013837 (2014).
- [69] L.-Z. Guo, A. Grimsmo, A. F. Kockum, M. Pletyukhov, and G. Johansson, “Giant acoustic atom: A single quantum system with a deterministic time delay,” *Phys. Rev. A* **95**, 053821 (2017).
- [70] A. F. Kockum, G. Johansson, and F. Nori, “Decoherence-free interaction between giant atoms in waveguide quantum electrodynamics,” *Phys. Rev. Lett.* **120**, 140404 (2018).
- [71] A. F. Kockum, “Quantum optics with giant atoms—the first five years,” *International Symposium on Mathematics, Quantum Theory, and Cryptography*, , 125 (2020).

- [72] B. Kannan, M. J. Ruckriegel, D. L. Campbell, A. F. Kockum, J. Braumüller, D. K. Kim, M. Kjaergaard, P. Krantz, A. Melville, B. M. Niedzielski, A. Vepsäläinen, R. Winik, J. L. Yoder, F. Nori, T. P. Orlando, S. Gustavsson, and W. D. Oliver, “Waveguide quantum electrodynamics with superconducting artificial giant atoms,” *Nature (London)* **583**, 775 (2020).
- [73] W. Zhao and Z. Wang, “Single-photon scattering and bound states in an atom-waveguide system with two or multiple coupling points,” *Phys. Rev. A* **101**, 053855 (2020).
- [74] L. Du, Y.-T. Chen, and Y. Li, “Nonreciprocal frequency conversion with chiral Λ -type atoms,” *Phys. Rev. Research* **3**, 043226 (2021).
- [75] Y.-X. Zhang, C. Carceller, M. Kjaergaard, and A. S. Sørensen, “Charge-noise insensitive chiral photonic interface for waveguide circuit QED,” *Phys. Rev. Lett.* **127**, 233601 (2021).
- [76] C. Wang, X.-S. Ma, and M.-T. Cheng, “Giant atom-mediated single photon routing between two waveguides,” *Opt. Express* **29**, 40116 (2021).
- [77] L. Du, Y.-T. Chen, Y. Zhang, and Y. Li, “Giant atoms with time-dependent couplings,” *preprint arXiv:2201.12575* (2022).
- [78] L.-Z. Guo, A. F. Kockum, F. Marquardt, and G. Johansson, “Oscillating bound states for a giant atom,” *Phys. Rev. Research* **2**, 043014 (2020).
- [79] T. Ozawa, H. M. Price, A. Amo, N. Goldman, M. Hafezi, L. Lu, M. C. Rechtsman, D. Schuster, J. Simon, O. Zilberberg, and I. Carusotto, “Topological photonics,” *Rev. Mod. Phys.* **91**, 015006 (2019).
- [80] M. Hafezi, E. A. Demler, M. D. Lukin, and J. M. Taylor, “Robust optical delay lines with topological protection,” *Nat. Phys.* **7**, 907–912 (2011).
- [81] D. L. Underwood, W. E. Shanks, Jens Koch, and A. A. Houck, “Low-disorder microwave cavity lattices for quantum simulation with photons,” *Phys. Rev. A* **86**, 023837 (2012).
- [82] A. A. Houck, H. E., and J. Koch, “On-chip quantum simulation with superconducting circuits,” *Nature Physics* **8**, 292–299 (2012).
- [83] X. Wang and H.-R. Li, “Chiral quantum network with giant atoms,” *Quantum Sci. Technol.* **7**, 035007 (2022).
- [84] D. F. James and J. Jerke, “Effective hamiltonian theory and its applications in quantum information,” *Can. J. Phys.* **85**, 625 (2007).
- [85] X. Gu, A. F. Kockum, A. Miranowicz, Y.-X. Liu, and F. Nori, “Microwave photonics with superconducting quantum circuits,” *Phys. Rep.* **718–719**, 1 (2017).
- [86] C. Weitenberg and J. Simonet, “Tailoring quantum gases by floquet engineering,” *Nat. Phys.* **17**, 1342–1348 (2021).
- [87] J. R. Johansson, P. D. Nation, and F. Nori, “Qutip: An open-source Python framework for the dynamics of open quantum systems,” *Comput. Phys. Commun.* **183**, 1760 (2012).
- [88] J. R. Johansson, P. D. Nation, and F. Nori, “Qutip 2: A Python framework for the dynamics of open quantum systems,” *Comput. Phys. Commun.* **184**, 1234 (2013).